TITLE
ASP Conference Series, Vol. **VOLUME**, **PUBLICATION YEAR**
EDITORS

Observations and models of the embedded phase of high-mass star formation

Floris F. S. van der Tak
Max-Planck-Institut für Radioastronomie, Auf dem Hügel 69, 53121 Bonn, Germany

Abstract. This paper is a review and an update on recent work on the physical and chemical structure of the envelopes of newly born massive stars, at the stages preceding ultracompact H II regions. It discusses methods and results to determine total mass, temperature and density structure, ionization rate, and depth-dependent chemical composition.

1. Introduction

The first major question in the study of high-mass star formation is whether or not the process is a scaled-up version of the formation of low-mass stars, which are known to form by accretion via a disk, and to disperse their natal envelopes through bipolar outflows. At the other extreme, high-mass stars may form by the coagulation of lower-mass stars or protostellar cores (see reviews by Churchwell and by Evans in this volume). The second major question of high-mass star formation is its relation to clustered star formation: does the stellar density influence the emergent mass spectrum? To what degree do the conditions in the initial molecular cloud determine the properties of the stellar population it produces?

The study of high-mass star formation is hampered by the short time-scale of the process. For example, a late O-type star lasts only $\sim$1 Myr, equal to the pre-main sequence lifetime of a 1 $M_\odot$ star. Moreover, 15% of this time is spent embedded in natal gas and dust that hides the photosphere from optical view. As a consequence, known regions of high-mass star formation lie at distances of several kpc, so that details $\lesssim$ 1000 AU are unresolved at typical $1''$ resolution. The large distances cause considerable confusion in these regions, and make it difficult to construct source samples with a common luminosity and distance, necessary for systematic studies.

To answer these questions, it is necessary to build up a statistically significant sample of regions forming high-mass stars, and to study their physical and chemical properties. This review describes recent studies of molecular material in which stellar groups including high-mass stars are forming. The focus is on detailed studies of small samples; larger source samples are described by Bronfman et al. (1996), Brand et al. (2001) and Sridharan et al. (2001). The first sample consists of nine deeply embedded objects of $L = 10^4 - 10^5$ $L_\odot$, $d = 1 - 4$ kpc, which have strong mid-infrared and weak cm-wave emission. The second set contains nine molecular clumps which have $L = 10^5 - 10^6$ $L_\odot$,

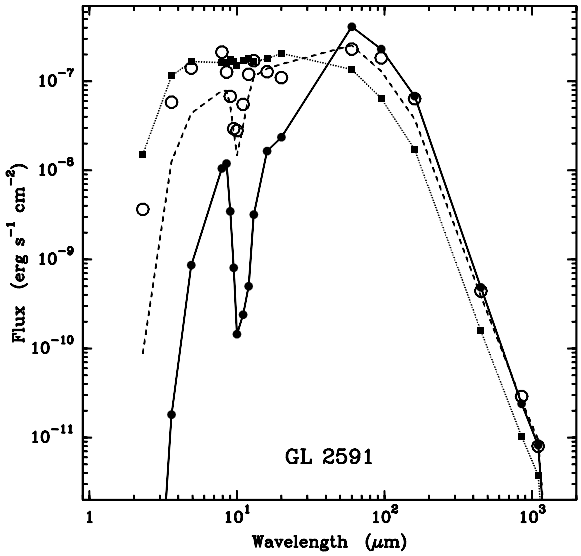

Figure 1. Spectral energy distribution of GL 2591. Open circles: data; solid line: model with coagulated dust grains and ice mantles; dashed line: model with coagulated dust grains but no ice mantles; dotted line: model with lower optical depth to fit the near-infrared. Based on: van der Tak et al. (1999).

$d = 4 - 14$ kpc and weak mid-infrared emission, and are close to ultracompact H II regions. Both samples are characterized by strong submillimeter continuum and line emission, associated H_2O and CH_3OH masers, and molecular outflows. In many cases, the distances are only kinematic estimates. Better distance estimates may come soon from near-infrared spectroscopy (Hanson et al. 1997; Kaper, this volume).

2. Physical structure

The determination of the physical structure of high-mass star-forming regions consists of two parts: first the measurement of the total mass and the temperature structure, and second the determination of the density structure.

2.1. Mass and temperature structure

The mass and temperature structure can be obtained by fitting dust models to the broad-band infrared spectrum. Masses derived from molecular line data are less reliable due to uncertain molecular abundances. As illustrated in Fig. 1 (solid line), a single model cannot fit the entire spectrum, so that to measure the mass, the model must be fitted to the optically thin part, at $\lambda \gtrsim 100\,\mu$m. Early models (Wolfire & Cassinelli 1986; Churchwell et al. 1990) mostly fitted the near-infrared part of the spectrum, which indicates $\sim$5 times lower optical depths than the submillimeter part due to deviations from spherical geometry. This result holds for both bright and weak mid-infrared sources (Harvey et al. 2000; Hatchell et al. 2000).

The source GL 2591 offers a rare opportunity to measure the submillimeter dust opacity by comparing dust masses to those derived from CO isotopic emission. While the CO mass is usually a lower limit since an unknown fraction of CO is frozen out onto dust grains, mid-infrared observations of GL 2591 indicate a ratio of gas-phase to solid-state CO column density of > 400 (Mitchell et al. 1989), reducing the uncertainty in CO abundance to better than a factor of two.

The dust masses of GL 2591 quoted in van der Tak et al. (1999) for Draine and Lee (1984) and Mathis et al. (1983) dust are a factor of 8 too high due to the use of a grain size of $0.05\,\mu$m rather than $0.1\,\mu$m. However, the conclusion that the dust model of Ossenkopf & Henning (1994) matches the mass derived from $C^{17}O$ best is still valid. This model for dust in star-forming regions includes grain coagulation and the formation of ice mantles.

The derived temperature profile indicates $T >$100 K at $r <$1000 AU from the central star. Within this radius, ice mantles on the grains should have evaporated. The dotted line in Fig. 1 is a calculation using the coagulated grain model without ice mantles. This model clearly fits the mid-infrared part of the spectrum better than the model with ice mantles.

2.2. Density structure

The density structure can be derived either by fitting dust models to the spatial profile of dust continuum emission, or by fitting the line spectrum of a molecule with a high dipole moment (such as CS) that is sensitive to density. The first approach assumes that the grain optical properties do not vary with position; the second that the molecular abundance does not. While either assumption may be invalid, the methods can serve as tests of each other.

Van der Tak et al. (2000a) found the two methods to agree well for six embedded high-mass star-forming regions, while for a seventh, S 140, the assumption of a centrally heated envelope appeared invalid. The good agreement between the dust and CS results may have been fortuitous due to the use of a Gaussian beam shape. Models of the 350 μm dust emission profile of GL 2591 using the actually measured beam shape indicate an r^{-2} density profile, steeper than the r^{-1} profile found from CS (Mueller et al., this volume). If this result also holds for the SCUBA data and the other sources, it indicates a depletion of CS at small radii. The alternative explanation of enhanced dust emissivity at small radii is not predicted by dust models, in which the main effect would be ice mantle evaporation, which drops the opacity.

3. Ionization

The fractional ionization of molecular clouds controls both the influence of magnetic fields on their dynamics and their gas-phase chemistry. In regions shielded from ultraviolet starlight, the main source of ionization is by cosmic rays which produce H_3^+, followed by proton transfer reactions into HCO^+ and H_3O^+. Current best estimates of the cosmic-ray ionization rate ζ based on the abundances of OH and HD measured in visual absorption toward nearby diffuse clouds have a factor of ten uncertainty (Federman et al. 1996). An alternative approach using the abundances of HCO^+ and DCO^+ measured through millimeter emission lines towards nearby dark clouds is no more accurate due to uncertain and

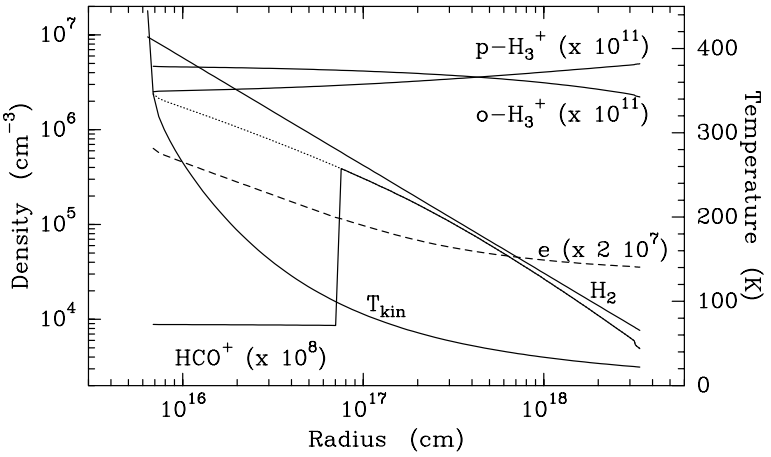

Figure 2. Density, temperature and ionization structure of GL 2136. The HCO^+ abundance drops at T=100 K due to reaction with evaporating H_2O ice. Based on van der Tak & van Dishoeck (2000).

potentially large depletion of CO and O (Caselli et al. 1998; Williams et al. 1998). At the current sensitivity, both these methods are limited to the solar neighbourhood and cannot give information on variations of ζ on Galactic scales.

The infrared H_3^+ detections (Geballe & Oka 1996; McCall et al. 1999) for well-characterized lines of sight make the embedded high-mass objects good targets for a more direct determination of ζ. Van der Tak & van Dishoeck (2000) combine the temperature and density structure of seven embedded sources with a small chemical network to compute their ionization structure (Fig. 2) and fitted the observed H_3^+ absorption and $H^{13}CO^+$ emission lines. The mean value of $\zeta = 2.6 \times 10^{-17}$ s^{-1} is consistent with the diffuse and dark cloud estimates, and with recent Voyager and Pioneer spacecraft data at distances of up to 60 AU from the Sun (Webber 1998). The source-to-source spread in ζ of a factor of 2-3 on scales of a few kpc agrees with results from $\gamma-$ray observations (Hunter et al. 1997). This agreement may be a coincidence since the $\gamma-$rays are of higher energy ($\sim$GeV) than the particles providing the bulk of the ionization (a few 10 MeV). Intervening clouds affect the H_3^+ but not the $H^{13}CO^+$ data.

Alternatively, the spread may be due to shielding against cosmic rays. The data suggest a trend of decreasing ζ with increasing total column density, but not at a significant level. However, HCO^+ probes the outer envelopes (Fig. 2), because in regions with $T > 100$ K, HCO^+ reacts with evaporating H_2O ice. Using tracers of the innermost parts of a low-mass core, Caselli et al. (2001) found $\zeta = 6 \times 10^{-18}$ s^{-1}. Follow-up studies may reveal by how much cosmic rays are attenuated inside dense cores.

4. Chemical stratification

The models described in § 2 have allowed us to study the chemical composition of the envelopes of embedded high-mass stars as a function of distance from the central star. The first example is the CH_3OH molecule studied by van der Tak et al. (2000b). Modeling of spectra indicates three types of sources (Fig. 3):

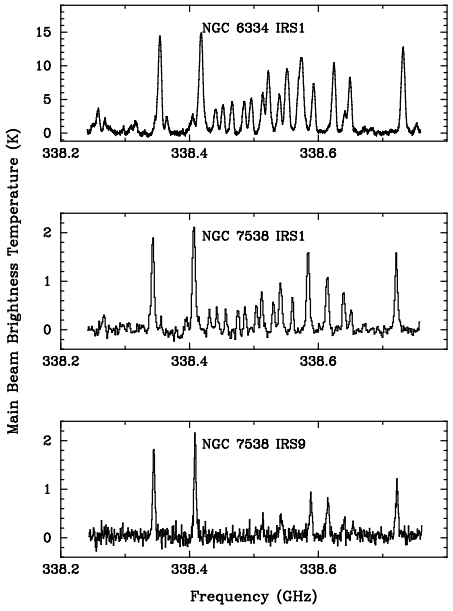

Figure 3. Spectra of the J=7-6 transition of CH_3OH at 338 GHz, taken with the JCMT, toward a 'cold', a 'jump' and a 'warm' source (bottom to top).

'cold' sources with $CH_3OH/H_2 \sim 10^{-9}$, 'warm' sources with $CH_3OH/H_2 \sim 10^{-8}$, and sources where the abundance 'jumps' from $\sim 10^{-9}$ to $\sim 10^{-7}$. This 'jump' occurs at $T \approx 100$ K, where solid H_2O, the bulk of icy grain mantles, evaporates. Combined with the high observed abundances of solid CH_3OH in these sources, these 'jumps' suggest an evolutionary sequence where CH_3OH forms on dust grains in 'cold' sources, then evaporates into the gas phase in 'jump' sources, and is broken down by reactions with ions in 'warm' sources. However, gas-phase CH_3OH abundances measured in the submillimeter are factors of $\gtrsim$100 lower than those derived from solid-state data. Since the nearby Orion region is an exception, resolution could play a role. Observations of gas-phase CH_3OH in infrared absorption with ground-based instruments with high spectral resolution may clarify this point.

A much earlier phase of evolution is probed by the CO molecule. Abundances derived from $C^{17}O$ line emission increase systematically by a factor of $\approx$3 as $\bar{T}$=20$\rightarrow$40 K, where $\bar{T}$ is the average temperature of the envelope, weighted by mass. Since these temperatures are the sublimation points of pure CO and mixed CO–H_2O ices, freeze-out and evaporation appear to control the CO abundance (van der Tak et al. 2000a). In low-mass cores, Kramer et al. (1999) found a similar relation of CO abundance with temperature. A third example of depth-dependent chemistry is the enhancement of HCN at temperatures $\gtrsim$ 300 K (Boonman et al. 2001). On the other hand, the abundance of H_2CO was found to be constant within the range $T = 20 - 240$ K, suggesting that this species is formed either in the gas phase or in CO-dominated ice. The latter idea is consistent with evidence from D_2CO (Ceccarelli et al. 2001).

The CO_2 molecule may be tracing the thermal history of star-forming regions. While the CO_2 ice abundance is high and evaporation of ices is observed,

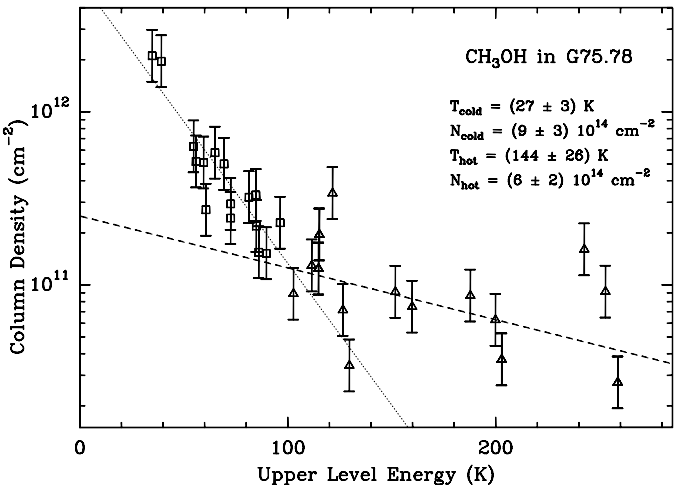

Figure 4. Rotation diagram of CH_3OH toward G75.78, a hot core close to an ultracompact H II region.

its gas-phase abundance is low, so that CO_2 must be rapidly destroyed after it evaporates (van Dishoeck 1998). However, there is no obvious low-temperature destruction path. The required $T \gtrsim 800$ K for CO_2 destruction is well above measured values, suggesting impulsive heating events in the past. Possibilities include outflow shocks (Charnley & Kaufman 2000), if desorption of the ices is also caused by these shocks. Other options are episodic accretion (Doty et al. 2001a) and the infrared flares discussed by Bally (this volume).

5. Envelope evolution

The evolution of the temperature and density structure of embedded objects was studied by van der Tak et al. (2000a). Conventional tracers of physical evolution, used for low-mass objects, do not change much over the narrow age range of the objects studied in detail. In particular, the shape of the spectral energy distribution does not change with time, as most material remains at low temperatures. The radio continuum flux does not seem indicative either, partly due to the unknown contribution of shocks, and partly because the surface temperatures of the ionizing stars are not well known.

However, the embedded objects can be ordered in a temperature sequence, based on the gas/solid ratios of H_2O and CO_2, the fraction of heated solid $^{13}CO_2$, the 45/100 μm colour, and the excitation temperatures of CO, C_2H_2 and CH_3OH. These indicators cover a wide range of temperatures and spatial scales, demonstrating that geometry is not an effect. Since crystallization is an irreversible process, the heated $^{13}CO_2$ ice measures the maximum temperature. Hence, the temperature change must be a systematic increase rather than random fluctuations, although gas-phase CO_2 argues the opposite. Still, the sequence may be evolutionary since it is correlated with the ratio of envelope mass to bolometric luminosity. If confirmed through a larger source sample, this correlation indicates the progressive dispersal of the envelope.

As for the time order of particular phenomena, the small body of existing data suggests that CH_3OH masers occur first, followed by H_2O masers, and later by OH masers. The situation is complex as each kind of maser may trace more than one physical component (Minier et al. 2001). Very massive and energetic outflows occur throughout the embedded phase, like for low-mass objects (Beuther, this volume).

The chemical composition of massive protostellar envelopes may serve as an independent probe of their structure and evolution. A good test case is GL 2591, for which a large body of data has been analyzed, both in submillimeter emission (JCMT, SWAS) and in infrared absorption (ISO-SWS, IRTF). Doty et al. (2001b) coupled the temperature and density structure of GL 2591 by van der Tak et al. (2000) to a complete gas-phase chemical network. It appears that the measured molecular abundances can be reproduced to within factors of a few for a source age of $\sim 3 \times 10^4$ yr.

6. Molecular gas near ultracompact H II regions

The results discussed so far pertain to a limited range of ages and luminosities. To see just how limited, we are investigating the set of line-rich molecular line sources near ultracompact H II regions from Hatchell et al. (1998). Observations of CH_3OH (Fig. 4) indicate the presence of both cold (20-50 K) and warm (110-500 K) gas. The column density ratio of these components ranges from <0.1 to >60, comparable to the values found in the embedded bright mid-infrared sources. The large implied masses of cold gas argue against a more evolved status of these regions, as would seem plausible based on their higher abundances of complex organic molecules. To analyze the data in more detail, we are developing models for the temperature and density structure, based on tracers of dust (SCUBA) and gas (CS lines).

7. Conclusions

Regions forming high-mass and low-mass stars have a different observational appearance, but their underlying structure and evolution seem similar. Regions forming massive stars are larger and hence more massive, but their absolute densities and their density distributions are similar to those found in low-mass star-forming regions. The more rapid dispersal of high-mass envelopes may be mainly driven by the faster pace of evolution of the central stars. There is mounting evidence for disks around high-mass stars, outflows are found to be ubiquitous, and compact dust and gas cores seem common as well.

The source samples with and without nearby ultracompact H II regions appear to evolve in parallel, suggesting that the proximity of radio emission and the shape of the spectral energy distribution are not good clocks. However, the excitation and abundance of selected molecules appear excellent tracers of evolution.

Acknowledgments. The author thanks Neal Evans and Ewine van Dishoeck for comments on this paper.

References

Boonman, A. M. S., Stark, R., van der Tak, F. F. S., et al. 2001, ApJ, 553, 63

Brand, J., Cesaroni, R., Palla, F., Molinari, S. 2001, A&A, 370, 230

Bronfman, L., Nyman, L.-A., May, J. 1996, A&AS, 115, 81

Caselli, P., Walmsley, C. M., Terzieva, R., Herbst, E. 1998, ApJ, 499, 234

Caselli, P., Walmsley, C. M., Zucconi, A., et al. 2001, ApJ, in press

Ceccarelli, C., Loinard, L., Castets, A., et al. 2001, A&A, 372, 998

Charnley, S. B., Kaufman, M. J. 2000, ApJ, 529, L111

Churchwell, E., Wolfire, M. G., Wood, D.O.S. 1990, ApJ, 354, 247

Doty, S.D., van Dishoeck, E.F., van der Tak, F.F.S., et al. 2001a, A&A, in press

Doty, S. D., van Dishoeck, E. F., van der Tak, F. F. S., Boonman, A. M. S. 2001b, A&A, submitted

Draine, B. T., Lee, H. M. 1984, ApJ, 285, 89

Federman, S. R., Weber, J., Lambert, D. L. 1996, ApJ, 463, 181

Geballe, T. R., Oka, T. 1996, Nature, 384, 334

Hanson, M.M., Howarth, I.D., Conti, P.S. 1997, ApJ, 489, 698

Harvey, P. M., Butner, H. M., Colomé, C., Di Francesco, J., Smith, B. J. 2000, ApJ, 534, 846

Hatchell, J., Fuller, G.A., Millar, T.J., Thompson, M.A., Macdonald, G.H. 2000, A&A, 357, 637

Hatchell, J., Thompson, M.A., Millar, T.J., Macdonald, G.H. 1998, A&AS, 133, 29

Hunter, S. D., Bertsch, D. L., Catelli, et al. 1997, ApJ, 481, 205

Kramer, C., Alves, J., Lada, C. J., et al. 1999, A&A, 342, 257

Mathis, J. S., Mezger, P. G., Panagia, N. 1983, A&A, 128, 212

McCall, B. J., Geballe, T. R., Hinkle, K. H., Oka, T. 1999, ApJ, 522, 338

Minier, V., Conway, J. E., Booth, R. S. 2001, A&A, 369, 278

Mitchell, G. F., Curry, C., Maillard, J.-P., Allen, M. 1989, ApJ, 341, 1020

Ossenkopf, V., Henning, T. 1994, A&A, 291, 943

Sridharan, T.K., Beuther, H., Schilke, P., et al. 2001, ApJ, in press

van der Tak, F. F. S., van Dishoeck, E. F. 2000, A&A, 358, L79

van der Tak, F. F. S., van Dishoeck, E. F., Evans, N. J., II, Bakker, E. J., Blake, G. A. 1999, ApJ, 522, 991

van der Tak, F. F. S., van Dishoeck, E. F., Evans, N. J., II, Blake, G. A. 2000a, ApJ, 537, 283

van der Tak, F. F. S., van Dishoeck, E. F., Caselli, P. 2000b, A&A, 361, 327

van Dishoeck, E. F. 1998, Faraday Discussion 109, 31

Webber, W. R. 1998, ApJ, 506, 329

Williams, J. P., Bergin, E. A., Caselli, P., Myers, P. C., Plume, R. 1998, ApJ, 503, 689

Wolfire, M.G., Cassinelli, J.P. 1986, ApJ, 310, 207